Nanoscale

PAPER

View Article Online
View Journal | View Issue

Check for updates

Cite this: *Nanoscale*, 2023, **15**, 15268

Laser-irradiated carbonized polyaniline-N-doped graphene heterostructure improves the cyclability of on-chip microsupercapacitor†

Bharat Bhushan Upreti, Navpreet Kamboj and Ramendra Sundar Dey *

Laser-irradiated graphene-based heterostructures have attracted significant attention for the fabrication of highly conducting and stable metal-free energy storage devices. Heteroatom doping on the graphene backbone has proven to have better charge storage properties. Among other heteroatoms, nitrogen-doped graphene (NG) has been extensively researched due to its several advanced properties while maintaining the original characteristics of graphene for energy storage applications. However, NG is generally prepared *via* chemical vapor deposition or high temperature pyrolysis method, which gives low yield and has a complex operation route. In this work, first a polyaniline-reduce graphene oxide (PANI-rGO) heterostructure was prepared *via in situ* electrochemical polymerization, followed by the deposition process. In the next step, laser-irradiation process was employed to carbonize polyaniline as well as doping of nitrogen on the graphene film, simultaneously. For the very first time, laser-irradiated carbonization of PANI on NG (cPANI-NG) heterostructure was utilized for microsupercapacitor (MSC). The as-prepared cPANI-NG-MSC shows extremely high cycling stability with a capacitance enhancement of 135% of its initial capacitance after 70 000 continuous charge–discharge cycles. It is very interesting to know the origin of the capacitance enhancement, which results from the change of pyrrolic N in NG-MSC to the pyridinic and graphitic N. An on-chip NG-MSC exhibits an excellent charge storage capacitance of 43.5 mF cm^{-2} at a current density of 0.5 mA cm^{-2} and shows impressive power delivery at a very high scan rate of 100 V s^{-1}. The excellent rate capability of the MSC shows capacitance retention up to 70.1% with the variation of current density. This unique approach to fabricate NG-MSC can have a broad range of applications as energy storage devices in the electronics market, as demonstrated by glowing a commercial red LED.

Received 15th June 2023,
Accepted 26th August 2023

DOI: 10.1039/d3nr02862c

rsc.li/nanoscale

Published on 28 August 2023. Downloaded on 1/31/2025 5:00:20 AM.

Introduction

Graphene, a highly researched material of the 21st century, is used as a supercapacitor electrode material due to its good cycling stability and electrical conductivity.[1] Laser-irradiation (LI) technique is a very fast, efficient, cost-effective, and reagent-less method that was regressively utilized for the fabrication of highly conducting robust graphene film.[2] Laser-irradiated graphene (LIG) can be obtained by single pass laser impact and is able to perform the complementary venture as current-collector and active electrode material in metal-free microsupercapacitors (MSCs).[3–5] In 2014, Tour *et al.*, first demonstrated the formation of a three-dimensional (3D) laser-induced graphene film and fabricated the MSC device that showed a notable stability performance of 100 000 continuous galvanostatic charge/discharge (GCD) cycles with a capacitive retention of 100% and an areal capacitance of 2.32 mF cm^{-2} at a current density of 10 μA cm^{-2}.[6,7] To regulate the charge storage properties in graphene-based materials, heteroatom doping is preferred to modify the graphene structure and therefore the charge storage distribution. Several heteroatoms such as phosphorous (P), nitrogen (N), and boron (B) can be used to dope into the undifferentiated graphene structure in order to increase the electron density distribution.[8,9] However, N-doped graphene (NG) is preferred among others as it has Fermi level regulation, improved electron density, and similar atomic size, which is requisite for charge storage applications.[10] The combination of the lone pair electrons of nitrogen and the π-system of carbon atoms enhances chemical and physical properties.[11,12]

Several methods have been employed so far to synthesize N-doped graphene-based nanostructure and are classified as *in situ* and *ex situ* N-doping methods. The typical *in situ*

Institute of Nano Science and Technology (INST), Mohali-140306, Punjab, India. E-mail: rsdey@inst.ac.in

† Electronic supplementary information (ESI) available. See DOI: https://doi.org/10.1039/d3nr02862c

This journal is © The Royal Society of Chemistry 2023

Published on 28 August 2023. Downloaded on 1/31/2025 5:00:20 AM.

N-doping procedure is a bottom-up method that generally includes chemical vapor deposition (CVD),[13] arc-discharge,[14] biomass pyrolysis,[15] and solvothermal synthesis.[16–18] However, the *ex situ* N-doping method includes thermal annealing,[19] wet chemistry methods,[20] plasma treatment,[21] and ion implantation.[22] The main weakness of these methods are that they either require high temperature or multistep process with hazardous reagents.[23] Furthermore, low product yield, difficulties in scaling up, and insufficient N-doping make these methods unsuitable for practical applications.

On the other hand, polyaniline (PANI), an N-containing conductive polymer, has been extensively studied as an electrode material for the past few decades[24] because of its facile synthesis, compelling redox properties, and moderate environmental stability. Depending on their redox state, PANI exists in different forms; most reduced pale yellow leucoemeraldine to green emeraldine salt/base and highly oxidized violet pernigraniline form.[25,26] Among them, the emeraldine base form is considered to be the conductive one in its protonated state and the other two forms are insulating even after protonation.[27,28] The pseudocapacitive behavior of PANI is well suited as an energy storage material, but its stability during the charge/discharge cycle is always a concern.[29,30] The reasons for the unstable charge/discharge cycles are as follows: (i) ion insertion that leads to mechanical expansion, (ii) electrode material delamination, and (iii) fibrous morphology of the PANI.[31] The long-term charge/discharge process leads to a volume expansion effect, which unavoidably results in the poor electrochemical stability of the supercapacitor.[32,33] Moreover, PANI-based electrode materials failed to show satisfactory rate capability.[34] Therefore, although PANI-based supercapacitor exhibits high specific capacitance, due to its poor rate capability and inferior cycle life, it cannot be used for commercial applications.

Ramendra Sundar Dey

Dr Ramendra Sundar Dey is a Scientist at Institute of Nano Science and Technology, Mohali, India. Previously, he was a Hans Christian Ørsted postdoc fellow at DTU, Denmark. He received Ph.D. in Chemistry from IIT Kharagpur, India. He is involved in research in the field of electrochemistry of nanomaterials focusing on energy storage, conversion, electrocatalysis, and ammonia synthesis. He has been honored with a number of prestigious National and International recognitions, like INSPIRE Faculty Award, Journal of Materials Chemistry A Emerging Investigator *and* ACS Applied Energy Materials Early Career Energy Scientists*. He is Associate of IASc Bengaluru and member of INYAS, INSA.*

Therefore, to address this problem, it is necessary to develop a procedure that will give electrochemically stable PANI-graphene heterostructure with sufficient N-doping, lowered electrical resistance between PANI and graphene, as well as a sufficient diffusion channel for the electrolyte. Herein, we report a novel N-doping strategy *via* the *in situ* electrochemical polymerization of PANI in the graphene network, followed by the laser-irradiation method, encouraging the nitrogen atoms to get bonded into the graphene network and converting the rGO-PANI heterostructure into a carbonized material (cPANI-NG). In order to synthesize a comparatively less stable pseudocapacitive material PANI to a highly stable cPANI-based EDLC material, a new and efficient strategy is introduced in this work. The new strategy not only helps to improve the cycling stability of the material but also enhances the specific capacitance value of LIG. We further fabricated an in-plane microsupercapacitor with the cPANI-NG material. The resulting on-chip cPANI-NG-MSC was very efficient in showcasing the unique capacitive behavior with extraordinary cycling life. Moreover, the developed devices have been extended in series and parallel connections to make a high-voltage module that can lighten up the available red LED bulb.

Experimental section

Synthesis of the PANI-rGO heterostructure film

Modified Hummers' method was used to synthesize graphene oxide (GO) reported in our previous reports.[35–37] Aniline was purified by the distillation process prior to use. The simultaneous *in situ* polymerization of aniline and simultaneous deposition of reduced graphene oxide (rGO) on copper foam (Cuf) substrate was carried out *via* a single-step chronoamperometric technique for 180 s at a potential of −1.1 V using copper foam (Cuf) as working, Pt as counter, and Ag/AgCl (3.5 M KCl) as reference electrode in the three-electrode system. Dispersion solution containing aniline (with different ratios 20, 15, 12, and 10 μL) and GO (3 mg mL^{-1}) in 20 mL 0.5 M $HClO_4$ and the final dispersion solution were named as 3GO/Aniline, 4GO/Aniline, 5GO/Aniline, and 6GO/Aniline, respectively. The detailed electrochemical deposition procedure has been explained in the ESI.† The as-deposited films from the different dispersion solutions were named as *x*rGO-PANI (where, x = 3, 4, 5, and 6, respective to the concentration of the dispersion solution). The prepared samples were transferred to 10% ammonium persulfate $(NH_4)_2S_2O_8$ solution (*x*rGO-PANI facing upwards) to etch out the supportive copper electrode. A freestanding *x*rGO-PANI film floats on the solution after Cu etches out completely. The film was then scooped with a plastic poly(terephthalate) (PET) sheet and then washed with DI water several times in order to remove any contamination and kept for drying overnight.

Carbonization of PANI through the laser irradiation (LI) method

LI technique was further utilized to reduce the partially reduced rGO film and simultaneous carbonizing PANI to dope

Published on 28 August 2023. Downloaded on 1/31/2025 5:00:20 AM.

N-atoms into the LIG network (as shown in Fig. 1) with a 10.6 μm wavelength, 24 W pulse power output, and 0.8 m s^{-1} speed of CO_2 laser source. The LI technique was strategically used to convert PANI to carbonized PANI and simultaneously converts rGO to N-doped graphene (NG). The resulting laser-irradiated graphene films prepared from different concentration ratios of aniline to GO dispersion solutions (3GO/Aniline, 4GO/Aniline, 5GO/Aniline, and 6GO/Aniline) were named as cPANI-NG_3, cPANI-NG_4, cPANI-NG_5, and cPANI-NG_6, respectively. The mechanism of the LI-based reduction is based on photomodulaion (photothermal oxidation/reduction) reaction.[38] In this LI method, laser irradiation creates a high local temperature (>2000 °C) on the laser spot, which helps to rearrange the C–C bonds after the removal of oxygen functionalities.[39] Moreover, the laser-irradiation of *x*rGO-PANI film helps to impregnate the N atoms of the graphene backbone. The high local temperature due to photothermal reaction is responsible for intramolecular dehydroxylation between PANI and neighboring carboxyl group.[40,41] The schematic representation of the mechanism is illustrated in Fig. 1.

Designing and modifying interdigitated microsupercapacitor (MSC)

A 1.06 μm near-infrared laser (NIR) was used to pattern the cPANI-NG film with a power output of 32 W, laser speed of 0.8 ms^{-1}, and 20 000 Hz frequency. The electrodes were patterned in parallel linear-shaped geometry in the dimensional ratio of length (800 μm) and width (500 μm). Finally, the as-fabricated parallel cPANI-NG electrodes were modified with a transparent polyvinyl alcohol (PVA) gel electrolyte, and the film

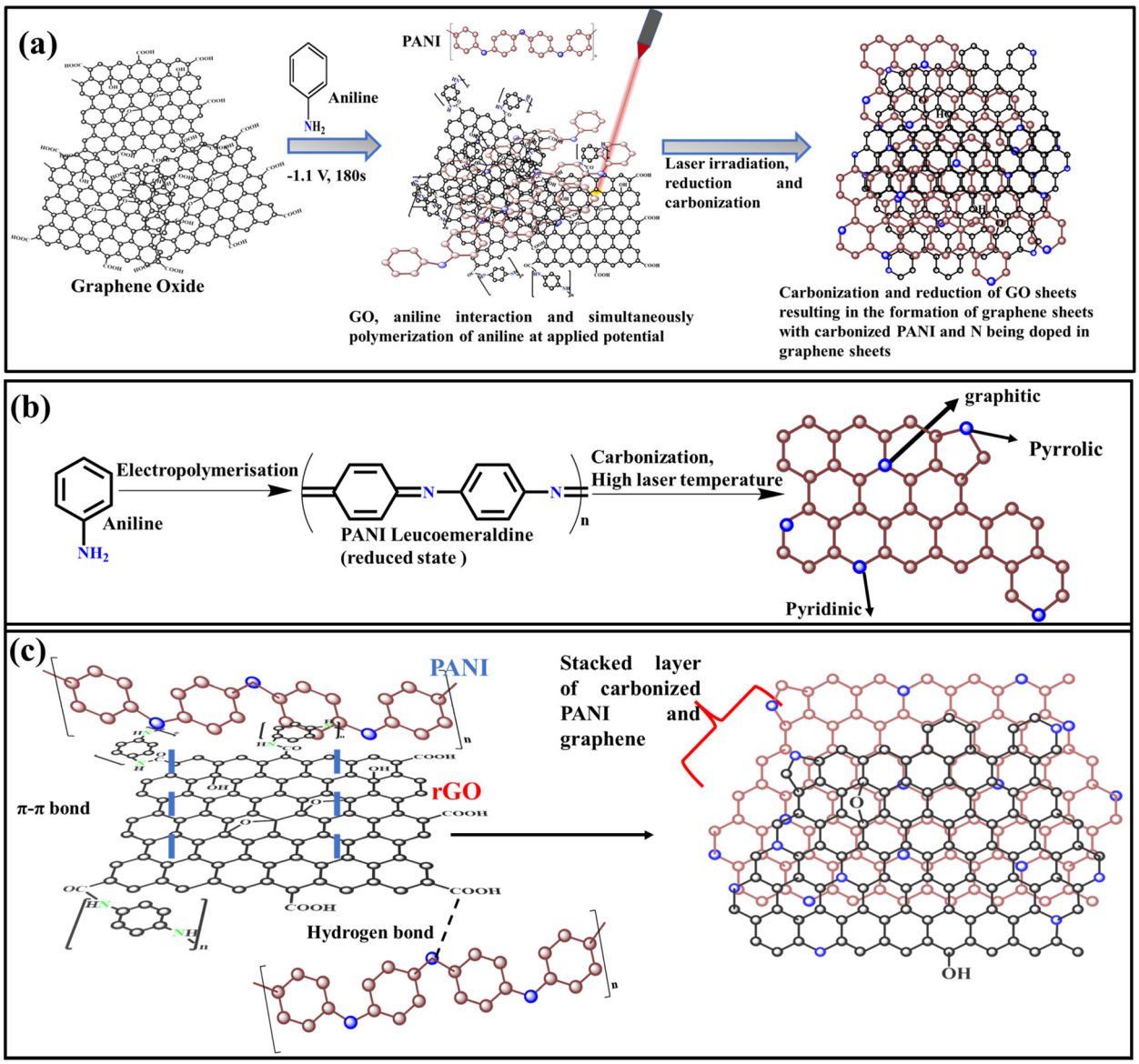

Fig. 1 (a) Schematic representation of carbonization of PANI and simultaneous N-doping of graphene; (b) mechanism of electropolymerization of PANI and (c) PANI carbonization and N-doping of graphene.

This journal is © The Royal Society of Chemistry 2023

Published on 28 August 2023. Downloaded on 1/31/2025 5:00:20 AM.

was kept overnight for drying in the vacuum condition. The modified film was named as carbonized polyaniline-N-doped graphene based microsupercapacitor (cPANI-NG-MSC) and directly used for further electrochemical studies.

Results and discussion

The synthesis of the cPANI-NG material involved two-step procedures, as shown in Fig. 1a. First, the polymerization of aniline was carried out, followed by the carbonization of the polymerized material. Moreover, upon laser irradiation, the PANI was converted to stack carbonized sheets and simultaneously electrochemically reduced graphene oxide sheet is converted to the N-doped graphene heterostructure (Fig. 1c). It is worth mentioning that during electrochemical polymerization, PANI makes composites with rGO, where PANI not only distributed over the rGO sheets due to π–π interaction but also acted as the linker between rGO sheets to form a network-like structure. After laser irradiation, the PANI gets converted into carbonized form (Fig. 1b) by losing nitrogen, which is simultaneously utilized in the doping of rGO and formed the cPANI-NG heterostructure.

To identify the functional groups present and the degree of reduction in the different electrode materials, Fourier-transform infrared (FT-IR) spectroscopy with attenuated total reflection (ATR) technique was performed on 3rGO-PANI, cPANI-NG_3, 4rGO-PANI, cPANI-NG_4, 5rGO-PANI, and cPANI-NG_5 samples, and the corresponding spectra are provided in Fig. S1, ESI† and Fig. 2a, respectively. The *in situ* polymerization of aniline under the applied potential leads to the formation of leucoemeraldine PANI, which is the reduced state of PANI.[26] The band at ~3200 cm^{-1} in the FT-IR spectra of *x*rGO-PANI in all ratios signifies the stretching frequencies for amine and –OH groups, which reduced significantly after laser irradiation.[42] Two other peaks at 1720 cm^{-1} and 1650 cm^{-1} appeared in case of the 4rGO-PANI sample (Fig. 2a), which is attributed to carbonyl C=O and amide peak, respectively.[43,44] It should be noted here that the amide linkage between PANI and rGO is favorable only when the pH of the electrolyte solution is very low, *i.e.*, the acidic media used for GO electrodeposition. After laser irradiation of the cPANI-NG_4 sample, the intensity of the peak at 1650 cm^{-1} corresponding to amide linkage reduced drastically (Fig. 2a), indicating the transformation of PANi to cPANI.

To understand the defect density, degree of graphitization, and crystalline nature of the samples, Raman spectroscopy was carried out for all the samples, such as LIG, cPANI-NG_3, cPANI-NG_4, and cPANI-NG_5, as shown in Fig. 2b. The G-band positioned in the range of 1575–1585 cm^{-1} corresponds to E_{2g} doubly degenerate phonons at the Brillouin zone, whereas the D-band in the range 1320–1355 cm^{-1} is attributed to the A_{1g} mode, which is related to the structural disorders and defects.[45] The intensity ratio of the G to D band (I_G/I_D) quantifies the defect density, which is directly related to nitrogen doping in LIG and the corresponding crystallite size. The I_G/I_D ratio was calculated for different samples and found to be 1.465 for LIG, 1.113 for cPANI-NG_5, 0.943 for cPANI-NG_4, and 1.180 for cPANI-NG_3. The I_G/I_D ratio in the case of cPANI-NG_4 sample confirms the formation of larger amount defects in comparison to other samples. The crystallite size was also calculated in all the samples, and the corresponding values are provided in the ESI Table S1.† The 2D-band that originates due to layered graphene-like structure almost disappeared in case of the cPANI-NG samples, which denotes the lower crystallinity of the NG samples,[46] as can be observed in Fig. 2b. Moreover, the full width at half maxima (FWHM) for the Raman spectra of the cPANI-NG material broadened, which also justifies the N-doping by replacing some graphitic carbons.[47,48] A slight shift of the G and D-bands in the doped graphene films towards the higher wavelength corresponds to the homogeneous incorporation of N atoms into the graphene structure at the atomic level. The degree of D and G band shifting depends on the N/C atomic ratios in the N-doped graphene film.[49] This band shifting also implies the presence of some specific types of N species, such as pyrrolic, pyridinic, and graphitic N, which can serve as electron acceptors.[50–52]

Further, to confirm the changes in the chemical composition of the samples, X-ray photoelectron spectroscopy (XPS) was conducted, as presented in Fig. 2c and d. The full survey XPS spectra of the cPANI-NG_4 sample shows C 1s, N 1s, and O 1s signals at binding energies of 285 eV, 401 eV, and 532 eV, respectively, indicating the presence of C, N, and O elements in the samples (Fig. S2, ESI†). The carbonization of PANI under laser impact leads to the N-doping, which was confirmed from the N 1s spectrum. High local temperature occurs due to photothermal reactions taking place during the laser irradiation process is responsible for more pyrrolic N after carbonization due to its greater thermal stability than the other forms of N.[53] The deconvoluted N 1s spectrum of cPAN-NG_4 shows that the appearance of pyridinic, pyrrolic, and graphitic

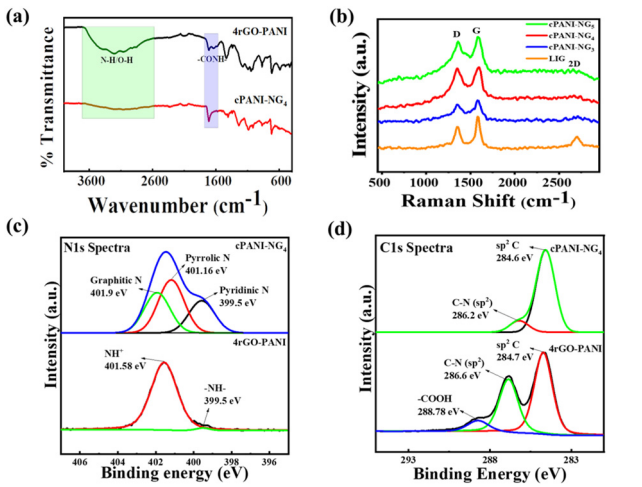

Fig. 2 (a) The FT-IR spectra of 4rGO-PANI and cPANI-NG_4, (b) Raman spectra of cPANI-NG_{3-5} and LIG samples, (c) and (d) shows N 1s and C 1s spectra of cPANI-NG_4 and 4rGO-PANI, respectively.

Published on 28 August 2023. Downloaded on 1/31/2025 5:00:20 AM.

nitrogen peaks corresponds to the binding energies of ~399.5 eV, ~401.2 eV, and ~401.9 eV, respectively, as shown in Fig. 2c.[54,55] These significant peaks for the N-doped graphene are absent but the peaks at 401.6 eV and 399.5 eV, which correspond to the Leucoemeraldine form of PANI, are present in the 4rGO-PANI film. The deconvoluted C 1s XPS spectra of cPANI-NG_4 and 4rGO-PANI are shown in Fig. 2d, which clearly depicts the presence of the N–sp^2-C peak positioned at a binding energy of 286.88 eV. Both the films represent the peak corresponding to the sp^2-C bond, which further signifies the aromatic system of PANI and carbon graphitic structure. The peak at 288.78 eV of the 4rGO-PANI sample is assigned for –COOH, which disappeared after laser-irradiation (as shown in Fig. 2d), confirming the reduction of the sample. The deconvoluted N 1s and C 1s spectra of 3rGO-PANI, cPANI-NG_3, 5rGO-PANI, and cPANI-NG_5 samples are also provided in Fig. S3 and S4, ESI.† The N 1s deconvoluted spectra of cPANI-NG_5 shows decreased graphitic N peak, suggesting that with increasing concentration of PANI, graphitic N decreases.

The carbonization of PANI into the graphene network develops irregular morphologies, which can be further investigated *via* scanning electron microscopy (SEM) and transmission electron microscopy (TEM) studies. Fig. 3a shows the SEM image of 4rGO-PANI (upper half portion) and cPANI-NG_4 (lower half portion) in a same sample distinct by a yellow dotted line. The SEM images depict that 4rGO-PANI has a rough crimpled morphology, as seen in Fig. 3b and c. The sheets get flattened and linked together after laser irradiation, which can be seen in Fig. 3d and e. Still, the presence of PANI induces defects to hinder the generation of a single joint sheet as observed in the case of only laser-irradiated graphene.[7] The HR-TEM studies of the cPANI-NG film in Fig. 3f shows the layered sheet structure of the as-prepared sample whereas 4rGO-PANI has few layers to multilayers sheet of large size, as seen in Fig. S5, ESI.† The TEM images reveal that after the laser irradiation, few layer graphene sheet-like structure is formed. The atomic percentages of C, O, and N are quantified using energy dispersive spectrometry (EDS) analysis in SEM, which shows that the nitrogen content is 10.3 atomic%, indicating that a sufficient amount of nitrogen has been doped on the graphene surface (Fig. S6, ESI†) compared to that of the 4rGO-PANI (Fig. S7, ESI†). The atomic percentage of nitrogen was 13.6%, suggesting that the laser irradiation has led to the removal some of the nitrogen-containing functionalities from the film. The elemental mapping of the cPANI-NG_4 sample was also performed, which confirmed the homogeneous distribution of oxygen, carbon, and nitrogen throughout the sample (Fig. 3g–j). Furthermore, the selected area electron diffraction (SAED) analysis (Fig. S8, ESI†) displays the absence of lattice points characteristic to the hexagonal lattice of crystalline graphene, which indicates that the crystallinity is substantially decreased after N doping.

The electrical property study of the electrode material is very important for the electronic transport investigation. The

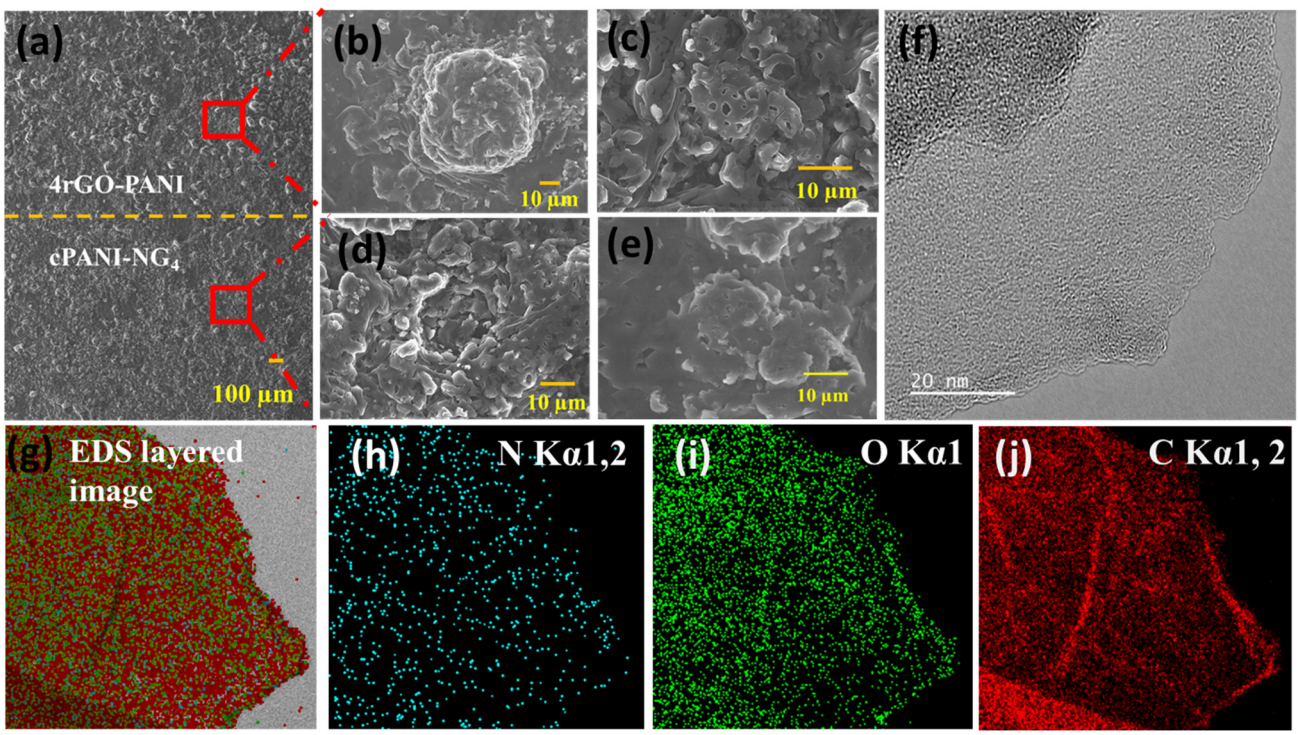

Fig. 3 (a) The SEM images of 4rGO-PANI and cPANI-NG_4 separated by a horizontal yellow line, (b) and (c) shows the morphology of 4rGO-PANI and laser-irradiated carbonized film cPANI-NG_4 morphology in (d) and (e), (f) shows the HRTEM image of the cPANI-NG_4 film. EDS of layered image (g) in TEM shows the content of N, O, and C in (h), (i), and (j) images, respectively.

 This journal is © The Royal Society of Chemistry 2023

Published on 28 August 2023. Downloaded on 1/31/2025 5:00:20 AM.

active material must possess high electrical conductivity for its use as supercapacitor; the *I–V* characteristic curve shows the ohmic behavior of the films, as shown in Fig. S9, ESI.† The conductivity of the 4rGO-PANI and cPANI-NG_4 films were measured by a two-probe method and calculated to be 478 S m^{-1} and 5933 S m^{-1}, respectively, which is comparatively higher than that of the activated carbon (10–100 S m^{-1}) and rGO (1000–2000 S m^{-1}) materials. Therefore, it can be concluded that the carbonization of PANI by the LI process helps to improve the restoration of π-electron clouds and endorse fast electron transport through the cPANI-NG_4 film.

Electrochemical characterization of MSC

The electrochemical polymerization of aniline has been well studied in the past few years. It is well known that at higher potential, the pernigraniline form of PANI hydrolyses in aqueous electrolyte, leading to the degradation of the polymer to oligomeric soluble units, which leads to the loss of capacity of the active material.[56,57] However, leucoemeraldine form, which is a highly reduced form of PANI, is formed when negative potential is applied. Therefore, the formation of pernigraniline can be avoided when a negative potential −1.1 V is applied during the *in situ* electrochemical deposition of GO and simultaneous polymerization of aniline. Fig. S10, ESI† shows the cyclic voltammetry (CV) response of the as-prepared 4rGO-PANI material in 1.5 M H_2SO_4 solution. The LI technique has been applied on rGO-PANI to synthesize a porous and conductive cPANI-NG material, as described in the Experimental section. It is interesting to note that the porous morphology of cPANI-NG allows the easy diffusion of ions whereas electronic flow is accelerated through the conductive graphene-based network (as visualized in Fig. 4a). In order to check the energy storage properties, the cPANI-NG materials prepared by different ratio of starting materials were electrochemically characterized to comprehend the effect of diffusion channels that were developed after the LI process. Cyclic voltammetry for all the samples (cPANI-$NG_{3,4,5,6}$) was carried out at a scan rate of 100 mV s^{-1} in aqueous 1 M H_3PO_4 solution in a three-electrode system (Fig. 4b). The CV curves are nearly rectangular in shape with larger area, suggesting better charge storage property of the materials. In comparison to other samples, cPANI-NG_4 exhibited the largest area under the curve resembling the highest capacitance; thus, it is chosen as optimized electrode materials for further electrochemical studies.

A solid-state parallel linear-shaped geometry cPANI-NG_4 based microsupercapacitor was designed and electrochemically characterized *via* different electrochemical techniques such as cyclic voltammetry (CV), galvanostatic charge/discharge (GCD), and electrochemical impedance spectroscopy (EIS) analysis. The CV curves at different scan rates (Fig. 4c) and GCD profiles at different current densities are shown in Fig. 4c and d, respectively. The EDLC behavior of the CV curve in Fig. 4c indicates that most of the PANI polymers are carbonized in the film or get fused with the graphene layer or form

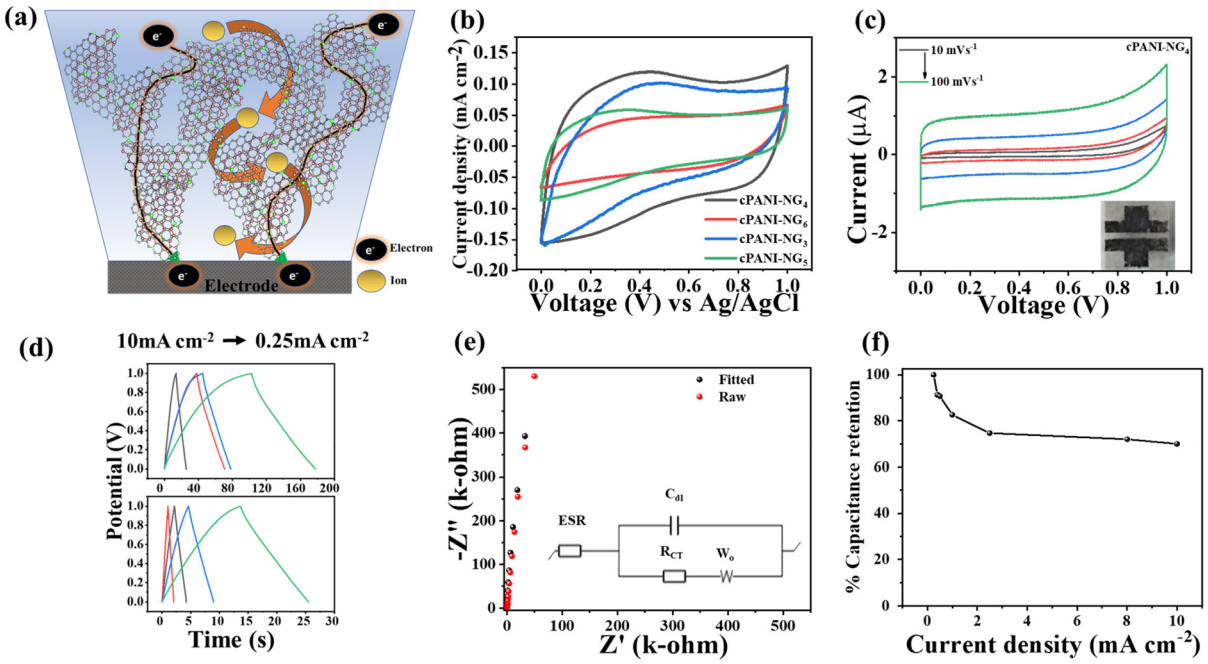

Fig. 4 (a) Schematic representation of the electron and ion transport between electrode–electrolyte interface. (b) CV curves for all the samples (cPANI-NG_3, cPANI-NG_4, cPANI-NG_5, cPANI-NG_5) in three-electrode system. (c) CV curves of cPANI-NG-MSC at different scan rates in 1 M H_3PO_4, inset shows the digital image of the device. (d) Galvanostatic charge–discharge (GCD) profile of cPANI-NG-MSC at different current densities. (f) Nyquist plot of cPANI-NG-MSC, inset shows the Randles equivalent circuit. (f) Capacitance retention *versus* current density plot showing the rate capability of cPANI-NG_4-MSC.

Published on 28 August 2023. Downloaded on 1/31/2025 5:00:20 AM.

N-doped graphene. PANI is an electroactive conducting polymer, which shows pseudocapacitive response (Fig. S10, ESI†), but after the LI process, its carbonized form displays electric double-layer capacitor (EDLC) type behavior, demonstrating superior charge storage property of the material. The CV curve at different scan rates from 10 to 100 mV s^{-1} shows perfect rectangular shape, retaining the EDLC behavior of the film (Fig. 4c). Fig. 4d illustrates the GCD profile of the device with varying current density from 10 to 0.25 mA cm^{-2}. The specific capacitance (C_{sp}) of the device was calculated from the GCD curve and found to be 43.5 mF cm^{-2} at a current density of 0.25 mA cm^{-2}. The electrochemical impedance spectroscopy (EIS) measurement was carried out to further understand the ease of ionic transport and capacitive nature of the device in the frequency range of 0.01 Hz to 100 kHz at an AC amplitude of 0.5 V. The Nyquist plot with its fitted curve (inset shows corresponding Randles Equivalent Circuit) shows a vertical line almost parallel to the *Y*-axis in the lower frequency region, which demonstrates perfect double layer formation by the cPANI-NG-MSC device (Fig. 4e). The parameters of the Randles circuit determined by the curve fitting of Nyquist plot are mentioned in Table S2, ESI.† The maximum area normalized energy density (E_A) and power density (P_A) of the cPANI-NG-MSC were calculated to be 1.95 m Wh cm^{-2} and 4.96 W cm^{-2}, respectively and the corresponding Ragone plot for the device is provided in Fig. S11, ESI.†

Generally, the specific capacitance of a supercapacitor decreases with increasing scan rate or increasing current densities, causing poor rate capabilities. The rate capability of the prepared cPANI-NG_4-based MSC was determined with the capacitance retention *vs.* current density plot for cPANI-NG_4 at 0.25–10 mA cm^{-2}. The retention of the C_{sp} was 70.1% of its initial capacitance value (Fig. 4f). The rate capability of the MSC was further evaluated by operating CV from 200 mV s^{-1} to 500 V s^{-1}, as shown in Fig. 5a–f. The rectangular shape of the device was retained even at a very high scan rate of 100 V s^{-1} (Fig. 5e), indicating excellent power delivery of the device. There is a little distortion in the shape of the voltammogram at 500 V s^{-1}, as shown in Fig. 5f. This study shows the fast formation of the adsorption layer on the surface of the film; as a result, instantaneous power delivery can be obtained.

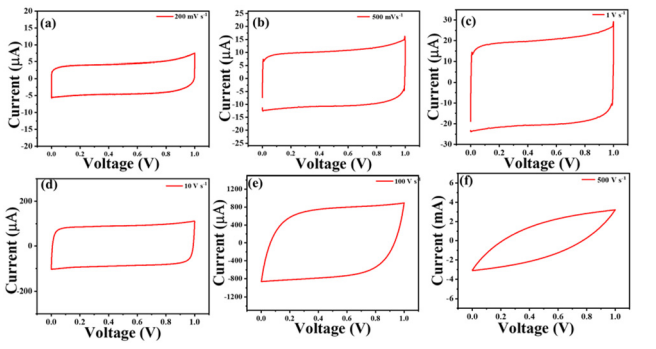

Fig. 5 CV curves of cPANI-NG-MSC at different scan rates (a) 200 mV s^{-1}, (b) 500 mV s^{-1}, (c) 1 V s^{-1}, (d) 10 V s^{-1}, (e) 100 V s^{-1}, and (f) 500 V s^{-1}, respectively.

The cycling stability is another one important factor of the energy storage system for the commercial feasibility of the device. The cycling performance of the device was examined under continuous long-term charge–discharge (CD) cycles. Generally, pseudocapacitive material such as PANI shows the degradation of the capacitance in the longer period CD cycles as the polymer contraction and expansion weakens the charge storage tendency of the material.[33] The cycling performance of the cPANI-NG MSC was examined using the galvanostatic charge–discharge cycling in the potential window of 0–1 V at a current density of 2 mA cm^{-2} for 70 000 continuous cycles, as shown in Fig. 6a. The inset of the Fig. 6a shows the retained triangular CD profile in different time intervals, showing the extraordinary stability of the cPANI-NG-MSC device in long run cycling. Interestingly, the device preserved almost 100% of coulombic efficiency during the cycling. It is stimulating to note that the MSC device shows an increase in the specific capacitance of up to 135% of the initial capacitance value after 70 000 cycles. The enhancement in the capacitance value after cycling can be explained by considering the nature of doped-nitrogen present in the laser-irradiated N-doped graphene film. In case of N-doped graphene, the total capacitance is obtained from the contribution of electric double layer capacitance (C_{EDL}) and the quantum capacitance (C_q). Ignoring the polarization effect of the electrode surface, the quantum and EDL capacitance can be considered separately for studying the total capacitance.[58–60] Amongst the different forms of N present in the material, namely, graphitic, pyridinic, and pyrrolic, graphitic and pyridinic nitrogen enhance the total capacitance by increasing the quantum capacitance, whereas the pyrrolic nitrogen limits the increase in total capacitance.[61] In this case, we observed that the enhancement in C_{sp} is up to 50 000 cycles, and the C_{sp} was stable up to 70 000 cycles. This enhancement corresponds to the decrease in the pyrrolic N present in the sample and enhancement of the pyridinic and graphitic N during GCD cycling. To prove this, XPS study was performed with the sample before and after the cycling test. The XPS study reveals that the area under the curve for pyrrolic N is more in comparison to the pyridinic and graphitic N for the sample before stability, whereas the same is decreased after stability, and the intensity of pyridinic N is increased after stability, as shown in Fig. 6b–d. The CV plot at 100 mV s^{-1} of cPANI-NG_4 before and after cycling stability is shown in Fig. S12, ESI.† As expected, the area under the curve after cycling stability is greater than the initial capacitance, which is due to increased capacitance value during cycling, corroborating the results obtained from the GCD study.

In order to meet the commercial requirement for current and/or voltage output, it is necessary to check the response of MSC devices in-series and in-parallel connection. Identical cPANI-NG_4 MSC devices are connected in series and parallel combination in order to meet the energy and power density requirement of the device. The MSC devices connected in series show increment in the operating voltage from 1 V to 2 V

 This journal is © The Royal Society of Chemistry 2023

Published on 28 August 2023. Downloaded on 1/31/2025 5:00:20 AM.

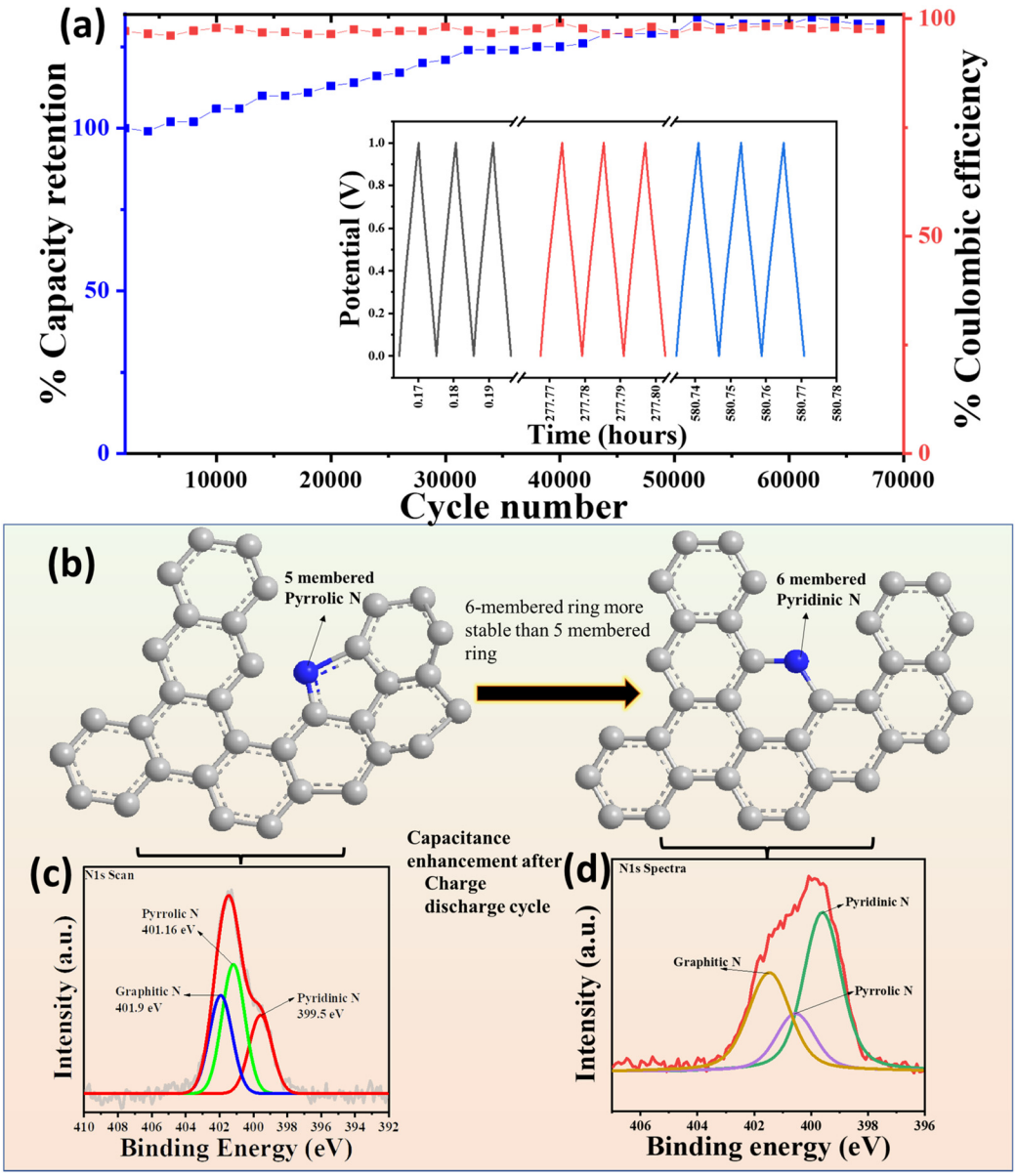

Fig. 6 (a) Plot of capacity retention and coulombic efficiency with the cycle number showing the long-life cycling stability of the cPANI-NG-MSC. (b) Enhancement in the capacitance during the long charge–discharge cycle is explained with the conversion of the 5-membered pyrrolic N to the 6-membered graphitic of pyridinic N. (c) and (d) show the N 1s XPS spectra before and after charge–discharge cycles, confirming the conversion of nitrogen.

and 3 V when two and three devices are connected in series configuration, respectively. However, as expected, when the devices are connected in parallel, a stepwise increment in the output current is observed. The GCD profile and CV plots of series and parallel connections of the devices are represented in Fig. 7. Fig. 7a shows the GCD profile with the increasing series connections of the devices, which shows the increase in the cell voltage up to 3 V, and the corresponding CV curves for the series combination is given in Fig. 7b. The three devices in series combination were extended in the parallel configuration as 3S × *y*P, where *y* = 1, 2, 3. The CV and GCD curves for different series and parallel configurations of devices is shown in Fig. 7c and d, and the corresponding digital image is shown in Fig. 7e. A comparative tabular representation with different parameters of our work and other reported works involving PANI and graphene (or carbon)-based MSCs is given in Table S3, ESI.† The comparison shows the superiority of the cPANI-NG material other than PANI-based supercapacitors. To demonstrate the use of cPANI-NG-MSC for commercial purpose, the ability of the device was validated by glowing a commercial LED. The MSC devices was patterned in 3S × 2P (Fig. 7e) configurations and was fully charged to 3 V for 3 minutes using a commercial DC power supply source, as shown in Fig. 7f. The module can lighten up a commercial 1.5

Published on 28 August 2023. Downloaded on 1/31/2025 5:00:20 AM.

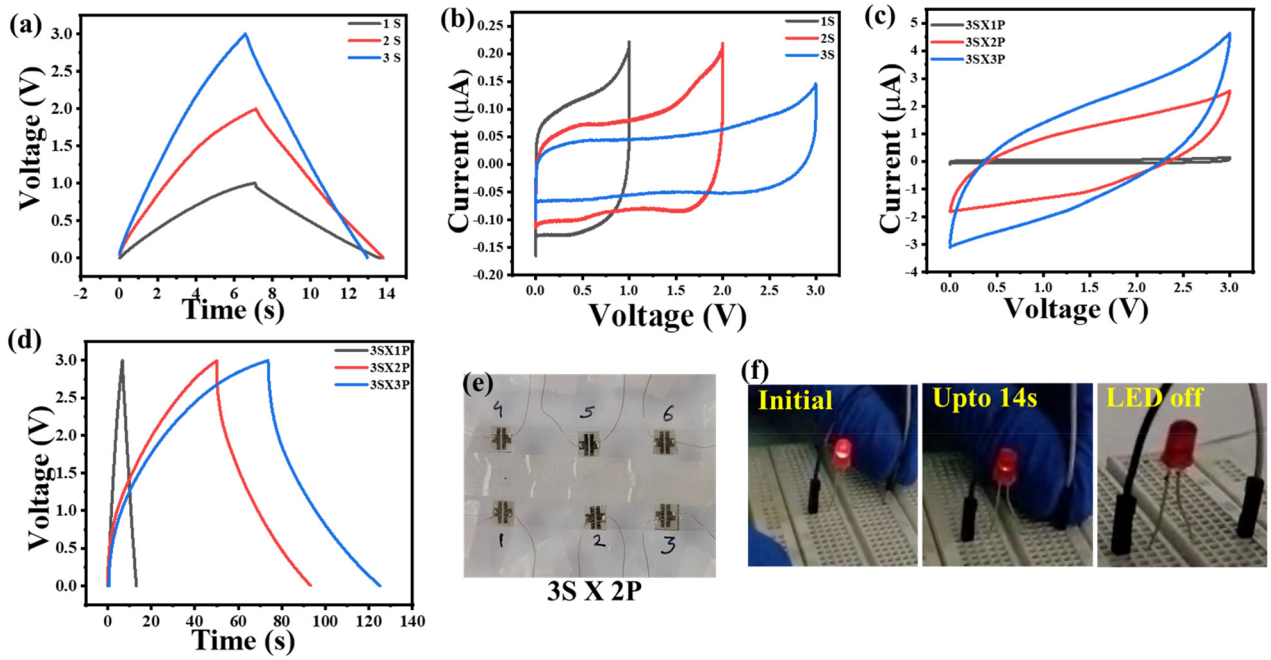

Fig. 7 (a) GCD curve of cPANI-NG-MSC connected in series (1S to 3S) at a current of 1 mA, (b) CV curves cPANI-NG-MSC in series combination (1S to 3S), (c) and (d) shows the CV curves and GCD curves of cPANI-NG-MSC connected in form 3S × 1P, 3S × 2P, and 3S × 3P. (e) Digital image showing connection 3S × 2P. (f) Digital image of commercial 1.5 V red LED lightened up using 3S × 2P cPANI-NG-MSC.

V LED, demonstrating the practical viability of the homemade in-plane microsupercapacitor.

Conclusions

In conclusion, in-plane microsupercapacitor is prepared by the laser irradiation of co-electrodeposited rGO-PANI freestanding film. The negative potential electrodeposition of the aniline favors the formation of the leucoemeraldine form. The LI method was impactful to convert pseudocapacitive PANI to the carbonized PANI and N-doped graphene that not only shows EDLC behavior but also offers high stability of the device. The device shows capacitance retention of 70.1% when the current density was varied from 0.25 to 10 mA cm^{-2}. The device shows high charge–discharge cycling stability of about 70 000 cycles with an enhancement of capacitance up to 135% of the initial value. During continuous charge–discharge cycles, the pyrrolic nitrogen formed after the laser irradiation slowly converted into the pyridinic and graphitic nitrogen, which is responsible for the increased capacitance of the device during cycling. The commercial viability of the device is established by lighting up the commercially available red LED.

Author contributions

R. S. D. designed the work; B. B. U. carried out all the experiments, data plotting, and wrote the first draft of manuscript, N. K. helped in data analysis and corrected the manuscript. R. S. D. supervised the work and corrected the manuscript. All the authors have discussed the results and assisted during the manuscript preparation, checked the final version of the manuscript, and approved it for submission.

Conflicts of interest

There are no conflicts to declare.

Acknowledgements

B. B. U. acknowledges INST Mohali for providing instrumental support and fellowship. N. K. acknowledges INST Mohali. R. S. D. acknowledges the DST SERB (CRG/2020/005683) funding agency for financial support.

References

1 Y. Wang, Z. Shi, Y. Huang, Y. Ma, C. Wang, M. Chen and Y. Chen, *J. Phys. Chem. C*, 2009, **113**, 13103–13107.
2 P. Huang, C. Lethien, S. Pinaud, K. Brousse, R. Laloo, V. Turq, M. Respaud, A. Demortiere, B. Daffos, P. L. Taberna, B. Chaudret, Y. Gogotsi and P. Simon, *Science*, 2016, **351**, 691–695.
3 Z. Peng, R. Ye, J. A. Mann, D. Zakhidov, Y. Li, P. R. Smalley, J. Lin and J. M. Tour, *ACS Nano*, 2015, **9**, 5868–5875.
4 R. Ye, D. K. James, J. M. Tour, R. Ye, D. K. James and M. Tour, *Adv. Mater.*, 2019, **31**, 1803621.

 This journal is © The Royal Society of Chemistry 2023

Published on 28 August 2023. Downloaded on 1/31/2025 5:00:20 AM.

5 N. Kamboj, B. B. Upreti, N. Kumar and R. S. Dey, *ACS Sustainable Chem. Eng.*, 2023, **11**, 5451–5461.
6 J. Lin, Z. Peng, Y. Liu, F. Ruiz-Zepeda, R. Ye, E. L. G. Samuel, M. J. Yacaman, B. I. Yakobson and J. M. Tour, *Nat. Commun.*, 2014, **5**, 5714.
7 N. Kamboj, T. Purkait, M. Das, S. Sarkar, K. S. Hazra and R. S. Dey, *Energy Environ. Sci.*, 2019, **12**, 2507–2517.
8 X. Wang, X. Li, L. Zhang, Y. Yoon, P. K. Weber, H. Wang, J. Guo and H. Dai, *Science*, 2009, **324**, 768–771.
9 S. Flandrois, B. Ottaviani, A. Derre and A. Tressaud, *J. Phys. Chem. Solids*, 1996, **57**, 741–744.
10 D. Wei, Y. Liu, Y. Wang, H. Zhang, L. Huang and G. Yu, *Nano Lett.*, 2009, **9**, 1752–1758.
11 N. Bundaleska, J. Henriques, M. Abrashev, A. M. Botelho Do Rego, A. M. Ferraria, A. Almeida, F. M. Dias, E. Valcheva, B. Arnaudov, K. K. Upadhyay, M. F. Montemor and E. Tatarova, *Sci. Rep.*, 2018, **8**, 12595.
12 W. J. Gammon, O. Kraft, A. C. Reilly and B. C. Holloway, *Carbon*, 2003, **41**, 1917–1923.
13 R. Zan and A. Altuntepe, *J. Mol. Struct.*, 2020, **1199**, 127026.
14 T. V. Pham, J. G. Kim, J. Y. Jung, J. H. Kim, H. Cho, T. H. Seo, H. Lee, N. D. Kim and M. J. Kim, *Adv. Funct. Mater.*, 2019, **29**, 1905511.
15 X. Kong, Y. Zhu, H. Lei, C. Wang, Y. Zhao, E. Huo, X. Lin, Q. Zhang, M. Qian, W. Mateo, R. Zou, Z. Fang and R. Ruan, *Chem. Eng. J.*, 2020, **399**, 125808.
16 D. Deng, X. Pan, L. Yu, Y. Cui, Y. Jiang, J. Qi, W. X. Li, Q. Fu, X. Ma, Q. Xue, G. Sun and X. Bao, *Chem. Mater.*, 2011, **23**, 1188–1193.
17 P. Samanta, S. Ghosh, S. Shit, B. Landge, S. K. Mandal, S. Sinha, G. G. Dutta and T. Kuila, *Electrochim. Acta*, 2021, **388**, 138571.
18 A. Paul, S. Ghosh, H. Kolya, C. W. Kang, N. C. Murmu and T. Kuila, *Chem. Eng. J.*, 2022, **443**, 136453.
19 Z. H. Sheng, L. Shao, J. J. Chen, W. J. Bao, F. Bin Wang and X. H. Xia, *ACS Nano*, 2011, **5**, 4350–4358.
20 Y. Zhang, K. Fugane, T. Mori, L. Niu and J. Ye, *J. Mater. Chem.*, 2012, **22**, 6575–6580.
21 M. Rybin, A. Pereyaslavtsev, T. Vasilieva, V. Myasnikov, I. Sokolov, A. Pavlova, E. Obraztsova, A. Khomich, V. Ralchenko and E. Obraztsova, *Carbon*, 2016, **96**, 196–202.
22 C. Bie, H. Yu, B. Cheng, W. Ho, J. Fan, J. Yu, C. Bie, H. Yu, B. Cheng, J. Yu, J. Yu Foshan, W. Ho and J. Fan, *Adv. Mater.*, 2021, **33**, 2003521.
23 C. Bie, H. Yu, B. Cheng, W. Ho, J. Fan and J. Yu, *Adv. Mater.*, 2021, **33**, 2003521.
24 S. Bhadra, D. Khastgir, N. K. Singha and J. H. Lee, *Prog. Polym. Sci.*, 2009, **34**, 783–810.
25 A. G. MacDiarmid and A. J. Epstein, *Faraday Discuss. Chem. Soc.*, 1989, **88**, 317–332.
26 W. Wu, Z. Lin, H. Y. Shi, L. Lin, X. Yang, Y. Song, X. X. Liu and X. Sun, *Chem. Eng. J.*, 2022, **427**, 131988.
27 H. Wang, J. Lin and Z. X. Shen, *J. Sci.: Adv. Mater. Devices*, 2016, **1**, 225–255.
28 C. H. B. Silva, N. A. Galiote, F. Huguenin, É. Teixeira-Neto, V. R. L. Constantino and M. L. A. Temperini, *J. Mater. Chem.*, 2012, **22**, 14052–14060.
29 S. C. Huang, S. M. Huang, H. Ng and R. B. Kaner, *Synth. Met.*, 1993, **57**, 4047–4052.
30 K. Wang, H. Wu, Y. Meng and Z. Wei, *Small*, 2014, **10**, 14–31.
31 Z. Sun, J. Zhang, F. Ye, W. Wang, G. Wang, Z. Zhang, S. Li, Y. Zhou and J. Cai, *J. Power Sources*, 2019, **443**, 227246.
32 Y. Xie and X. Sha, *Synth. Met.*, 2018, **237**, 29–39.
33 C. Xia, W. Chen, X. Wang, M. N. Hedhili, N. Wei and H. N. Alshareef, *Adv. Energy Mater.*, 2015, **5**, 1401805.
34 A. Eftekhari, L. Li and Y. Yang, *J. Power Sources*, 2017, **347**, 86–107.
35 T. Purkait, G. Singh, D. Kumar, M. Singh and R. S. Dey, *Sci. Rep.*, 2018, **8**, 640.
36 R. S. Dey, H. A. Hjuler and Q. Chi, *J. Mater. Chem. A*, 2015, **3**, 6324–6329.
37 T. Purkait, G. Singh, N. Kamboj, M. Das and R. S. Dey, *J. Mater. Chem. A*, 2018, **6**, 22858–22869.
38 H. Zhang and Y. Miyamoto, *Phys. Rev. B: Condens. Matter Mater. Phys.*, 2012, **85**, 033402.
39 N. Kamboj, T. Purkait, M. Das, S. Sarkar, K. S. Hazra and R. S. Dey, *Energy Environ. Sci.*, 2019, **12**, 2507–2517.
40 P. E. Dyer, G. A. Oldershaw and J. Sidhu, *Appl. Phys. B: Photophys. Laser Chem.*, 1989, **48**, 489–493.
41 H. Hu, Q. Li, L. Li, X. Teng, Z. Feng, Y. Zhang, M. Wu and J. Qiu, *Matter*, 2020, **3**, 95–126.
42 R. Trusovas, G. Račiukaitis, G. Niaura, J. Barkauskas, G. Valušis and R. Pauliukaite, *Adv. Opt. Mater.*, 2016, **4**, 37–65.
43 S. Neelakandan, N. Jacob K, P. Kanagaraj, R. M. Sabarathinam, A. Muthumeenal and A. Nagendran, *RSC Adv.*, 2016, **6**, 51599–51608.
44 L. Ruangchuay, J. Schwank and A. Sirivat, *Appl. Surf. Sci.*, 2002, **199**, 128–137.
45 M. E. M. Buan, N. Muthuswamy, J. C. Walmsley, D. Chen and M. Rønning, *Carbon*, 2016, **101**, 191–202.
46 C. Zhang, L. Fu, N. Liu, M. Liu, Y. Wang, Z. Liu, C. H. Zhang, L. Fu, N. Liu, Z. F. Liu, M. H. Liu and Y. Y. Wang, *Adv. Mater.*, 2011, **23**, 1020–1024.
47 Q. H. Yang, P. X. Hou, M. Unno, S. Yamauchi, R. Saito and T. Kyotani, *Nano Lett.*, 2005, **5**, 2465–2469.
48 H. Deng, Q. Li, J. Liu and F. Wang, *Carbon*, 2017, **112**, 219–229.
49 J. H. Kaufman, S. Metin and D. D. Saperstein, *Phys. Rev. B: Condens. Matter Mater. Phys.*, 1989, **39**, 13053.
50 K. S. Subrahmanyam, A. K. Manna, S. K. Pati and C. N. R. Rao, *Chem. Phys. Lett.*, 2010, **497**, 70–75.
51 U. J. Kim, C. A. Furtado, X. Liu, G. Chen and P. C. Eklund, *J. Am. Chem. Soc.*, 2005, **127**, 15437–15445.
52 W. Gu, J. Liu, M. Hu, F. Wang and Y. Song, *ACS Appl. Mater. Interfaces*, 2015, **7**, 26914–26922.
53 H. M. Jeong, J. W. Lee, W. H. Shin, Y. J. Choi, H. J. Shin, J. K. Kang and J. W. Choi, *Nano Lett.*, 2011, **11**, 2472–2477.

54 D. Wei, Y. Liu, Y. Wang, H. Zhang, L. Huang and G. Yu, *Nano Lett.*, 2009, **9**, 1752–1758.
55 R. J. J. Jansen and H. van Bekkum, *Carbon*, 1995, **33**, 1021–1027.
56 Y. Xia, J. M. Wiesinger, A. G. MacDiarmid and A. J. Epstein, *Chem. Mater.*, 1995, **7**, 443–445.
57 Q. Zhang, A. Zhou, J. Wang, J. Wu and H. Bai, *Energy Environ. Sci.*, 2017, **10**, 2372–2382.
58 E. Paek, A. J. Pak and G. S. Hwang, *J. Chem. Phys.*, 2015, **142**, 024701.
59 E. Paek, A. J. Pak and G. S. Hwang, *J. Electrochem. Soc.*, 2013, **160**, A1–A10.
60 J. Vatamanu, X. Ni, F. Liu and D. Bedrov, *Nanotechnology*, 2015, **26**, 464001.
61 C. Zhan, Y. Zhang, P. T. Cummings and D. Jiang, *Phys. Chem. Chem. Phys.*, 2016, **18**, 4668–4674.

Published on 28 August 2023. Downloaded on 1/31/2025 5:00:20 AM.

This journal is © The Royal Society of Chemistry 2023